Toward a Quantitative Analysis of Association Reactions in the Atmosphere

Jürgen Troe

Institut für Physikalische Chemie, Universität Göttingen, Tammannstrasse 6, D-37077 Göttingen, Germany

Received March 5, 2003

Contents

1. Introduction 4565
2. High-Pressure Range 4568
3. Low-Pressure Range 4571
4. Falloff Range 4572
5. Radical Complex Mechanism 4575
6. Conclusions 4575
7. Acknowledgments 4576
8. References 4576

1. Introduction

Association reactions of atoms or radicals with other, mostly less reactive species, forming more or less stable "reservoir molecules", play an important role in atmospheric chemistry. Reaction cycles such as the O_x, HO_x, NO_x, and $HalO_x$ cycles are terminated by such processes. The concentrations of the active species in these cycles and, hence, their catalytic effectiveness depend on the rates of the association reactions. As a consequence, atmospheric lifetimes of natural and anthropogenic constituents of the atmosphere are directly concerned.

Examples for atmospheric association reactions are numerous.[1,2] The stratospheric Chapman mechanism is terminated by the formation of ozone

$$O + O_2 (+M) \rightarrow O_3 (+M)$$

where M stands for the full variety of third-body gases present in the atmosphere. Nitric acid is formed through

$$HO + NO_2 (+M) \rightarrow HONO_2 (+M)$$

The $HalO_x$ cycles (Hal, halogen atoms) lead to the appearance of $HalONO_2$ molecules

$$ClO + NO_2 (+M) \rightarrow ClONO_2 (+M)$$

$$BrO + NO_2 (+M) \rightarrow BrONO_2 (+M)$$

HO_2 is generated through

$$H + O_2 (+M) \rightarrow HO_2 (+M)$$

and can further combine with NO_2 to form

$$HO_2 + NO_2 (+M) \rightarrow HO_2NO_2 (+M)$$

Alkyl or partially oxidized alkyl radicals may combine with O_2, forming peroxy radicals which through combination with NO_2 lead to classes of PAN-related molecules.

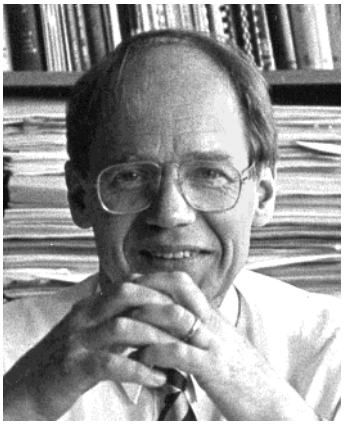

Jürgen Troe (born in 1940) received his Ph.D. at the University of Göttingen in 1965. He was Professor for Physical Chemistry at the Ecole Polytechnique Fédérale de Lausanne from 1971 to 1975. He then became Professor for Physical Chemistry at the University of Göttingen which he is still today. Since 1990, in addition, he has directed the Section for Spectroscopy and Photochemical Kinetics at the Max-Planck-Institute for Biophysical Chemistry at Göttingen. His activities, in experiment and theory, are centered around reaction kinetics, spectroscopy, photochemistry, atmospheric chemistry, and combustion. Since 1978, he has been a member of the IUPAC Subcommittee on Gas Kinetic Data Evaluation for Atmospheric Chemistry (see ref 1).

Association reactions are directly related to the reverse dissociation processes, some of which may also occur in the atmosphere. An example is the formation and thermal dissociation of N_2O_5 via

$$NO_2 + NO_3 (+M) \rightarrow N_2O_5 (+M)$$

$$N_2O_5 (+M) \rightarrow NO_2 + NO_3 (+M)$$

The rates of the association reactions do depend not only on the concentrations of the reactants and on the temperature but also on the concentration of the bath gases M and their chemical nature. This is generally explained by the classical energy transfer (Lindemann) mechanism which, for a process of the type

$$A + B + M \rightarrow AB + M$$

can be formulated symbolically in terms of the steps

$$A + B \rightarrow AB^* \quad (1)$$

$$AB^* \rightarrow A + B \quad (-1)$$

$$AB^* + M \rightarrow AB + M \quad (2)$$

With steady-state concentrations of AB*, this leads

10.1021/cr020514b CCC: $44.00
Published on Web 10/22/2003

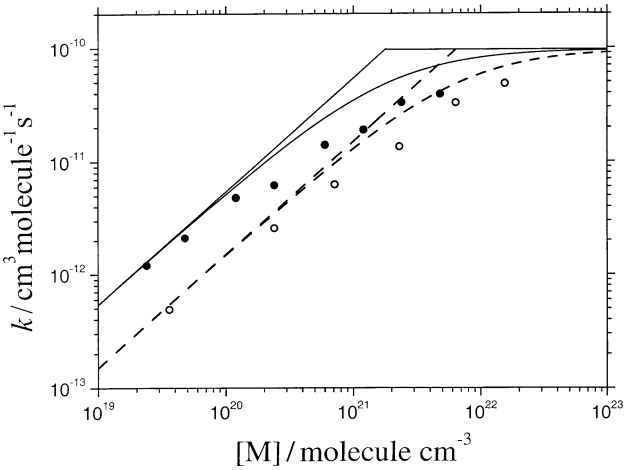

Figure 1. Second-order rate coefficients for the H + O_2 (+M) → HO_2 (+M) association reaction near 300 K: (●) M = N_2 and (○) M = He. Experimental data and estimated limiting rate coefficients are from ref 3; see the text.

to a rate expression

$$\frac{\mathrm{d[AB]}}{\mathrm{d}t} = k[\mathrm{A}][\mathrm{B}] \tag{3}$$

with a pseudo-second-order rate coefficient

$$k = k_1\left(\frac{k_2[\mathrm{M}]}{k_{-1} + k_2[\mathrm{M}]}\right) \tag{4}$$

Equation 4 is easily interpreted by identifying the maximum value of k with the rate constant k_1 for formation of the highly excited unstable adduct AB* and by identifying the parenthesis at the right-hand side of eq 4 with the fraction of AB* which is collisionally stabilized by reaction 2 rather then being redissociated via reaction −1.

Some atmospheric association reactions, such as the O + O_2 + M → O_3 + M, Cl + O_2 + M → ClOO + M, and ClO + ClO + M → Cl_2O_2 + M reactions, have been postulated to follow a different mechanism, the radical complex mechanism with the steps

$$\mathrm{A} + \mathrm{M} \rightarrow \mathrm{AM} \tag{5}$$

$$\mathrm{AM} \rightarrow \mathrm{A} + \mathrm{M} \tag{-5}$$

$$\mathrm{AM} + \mathrm{B} \rightarrow \mathrm{AB} + \mathrm{M} \tag{6}$$

See section 5. With an A + M ⇔ AM equilibrium, this leads to a rate coefficient of the form

$$k = \frac{k_6 K_5[\mathrm{M}]}{1 + K_5[\mathrm{M}]} \tag{7}$$

where $K_5 = k_5/k_{-5}$. Obviously, this mechanism has intrinsic properties different from those of the energy transfer mechanism, although it shows an analogous dependence of k on [M] and, therefore, may not be easily identified. For a distinction of the two mechanisms, see below.

In Figures 1−3, we show experimental results for the pressure dependences of three association reactions. We have chosen the H + O_2 (+M),[3] NO_2 + NO_3 (+M),[4−8] and HO + C_3H_6 (+M)[9,10] reactions as examples. Corresponding to eq 4, the pressure dependence is represented by the dependence of k on [M]. While all three curves show a transition from low-pressure third-order behavior (k proportional to [M]) to high-pressure second-order behavior (k independent of [M]), the change in reaction order occurs at quite different pressures or different M concentrations. The smaller the number of atoms in AB, the larger generally are the pressures required for approaching the high-pressure limit.

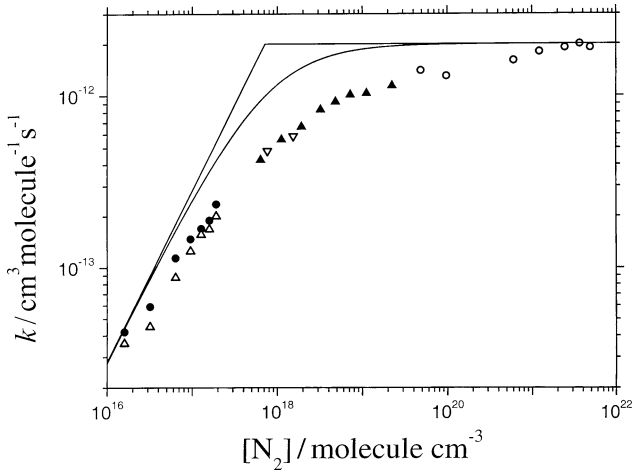

Figure 2. Second-order rate coefficients for the NO_2 + NO_3 (+N_2) → N_2O_5 (+N_2) association reaction near 300 K. Experimental data: (●) ref 4, (○) ref 5, (△) ref 6, (▽) ref 7, and (▲) ref 8. Estimated limiting rate constants are from refs 5 and 8; see the text.

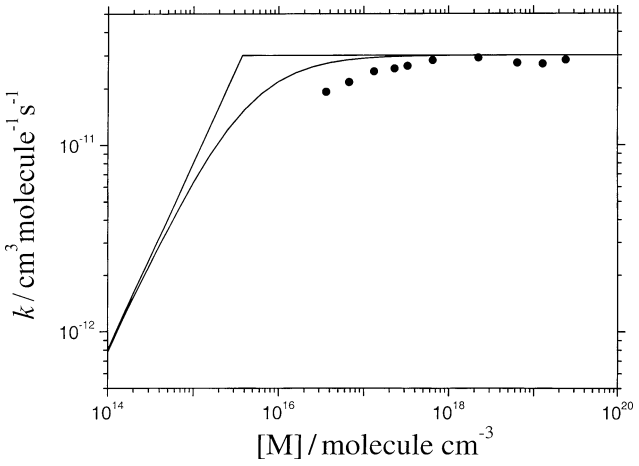

Figure 3. Second-order rate coefficients for the HO + C_3H_6 (+M) → HOC_3H_6 (+M) association reaction near 300 K (M corresponding to air, experimental data and estimated limiting rate coefficients from ref 10; see the text).

Although eq 4 qualitatively reproduces the behavior of Figures 1−3, it is well-known that it fails on a quantitative level. To demonstrate this, it is convenient[11] to choose a reduced form, representing k in terms of the limiting low- and high-pressure rate coefficients and an interpolation expression. At low pressures (k_2[M] ≪ k_{-1}), eq 4 approaches a limiting low-pressure rate coefficient

$$k_0 = \lim_{[\mathrm{M}]\rightarrow 0} k = k_2(k_1/k_{-1})[\mathrm{M}] \tag{8}$$

which corresponds to a third-order rate law with a

pressure-proportional second-order rate coefficient k. At high pressures (k_2[M] $\gg k_{-1}$), k approaches a limiting high-pressure rate constant

$$k_\infty = \lim_{[M]\to\infty} k = k_1 \tag{9}$$

which corresponds to a second-order rate law. The dependence of k on [M] is generally called the "falloff" curve because it describes the falloff of k below k_∞ when the pressure decreases. One may call that [M] the "center of the falloff curve" where k_2[M] = k_{-1}. Using k_0 and k_∞ from eqs 8 and 9, eq 4 can be rewritten as

$$k = \frac{k_0 k_\infty}{k_0 + k_\infty} \tag{10}$$

where k_0 is proportional to [M] and the center of the falloff curve is where $k_0 = k_\infty$. In the doubly reduced form, the falloff curve then is expressed by

$$\frac{k}{k_\infty} = \frac{k_0/k_\infty}{1 + k_0/k_\infty} \tag{11}$$

where k_0/k_∞ represents a reduced pressure scale. Comparing eq 11 with experimental results requires the knowledge of k_0 and k_∞ from measurements over sufficiently large pressure ranges or from accurate calculations as far as these are possible. Figure 2 allows for such a test, while Figures 1 and 3 do not provide data at sufficiently high and low pressures, respectively. One may also ask whether the two limits have been approached sufficiently well in Figure 2, but at least an empirical continuation of the experimental curves appears to be possible (for more details, see below). After k_0 and k_∞ have been chosen, as shown in Figures 1 and 2, the predictions from eq 4 are included in Figures 1 and 2. One notices that the experimental falloff curves are markedly below eq 4, the effect being more pronounced for the N_2O_5 system than for the HO_2 system. It has become customary to represent this effect by "broadening factors" $F(k_0/k_\infty)$,[11] to be introduced into eq 11

$$\frac{k}{k_\infty} = \frac{k_0/k_\infty}{1 + k_0/k_\infty} F(k_0/k_\infty) \tag{12}$$

In Figure 4, we try to extract the experimental broadening factors from Figures 1 and 2. Bell-shaped curves arise. However, their accurate details depend on the correct choice of k_0 and k_∞ (k_∞ for the HO_2 system was taken from ab initio calculations, see below; k_0 for the HO_2 system and k_0 and k_∞ for the N_2O_5 system were taken from the experiments). The "center broadening factors"

$$F_{cent} = F(k_0/k_\infty = 1) \tag{13}$$

in particular depend on the selected k_0 and k_∞: excessively small values of k_0 and k_∞ result in excessively large values of F_{cent}.

There are several reasons for the appearance of the F broadening factors in eq 12. First, the excited species AB* in the mechanism of reactions 1, −1, and 2 are formed in wide ranges of energies E and angular momenta (quantum numbers J); i.e., reaction steps 1 and −1 depend on E and J. Second, the collisional stabilization (eq 2) is a multistep process with sequences of de- and reactivating collisions between states with different E and J values which requires the formulation of a two-dimensional master equation. Handling the mentioned complications is the issue of modern unimolecular rate theory. It provides a theoretical access to the broadening factors $F(k_0/k_\infty)$ in comparison to the experimental results from Figure 4. The consideration of both, experiments and theories, is the obligatory condition for an understanding of the finer details of falloff curves such as those shown in Figures 1−3.

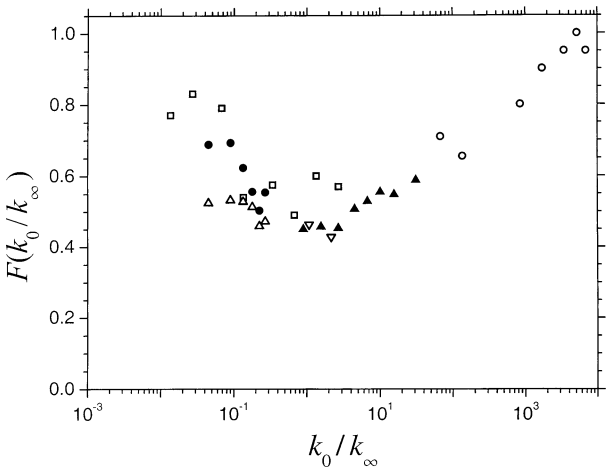

Figure 4. Experimental broadening factors $F(k_0/k_\infty)$ for the H + O_2 (+N_2) → HO_2 (+N_2) and NO_2 + NO_3 (+N_2) → N_2O_5 (+N_2) association reactions [experimental results from Figures 1 (□) and 2 (symbols as in Figure 2); see the text].

An economic representation of the complicated dependence of the pseudo-second-order rate coefficient k on the temperature T, the bath gas concentration [M], and the chemical nature of M is provided by suitable expressions for k_0, k_∞, and $F(k_0/k_\infty)$. Unfortunately, this procedure makes data evaluation and representation, as well as modeling of association reactions in atmospheric chemistry, more complicated than one would have liked. However, this problem cannot be avoided. The following review describes an approach to analyzing, predicting, and representing k_0, k_∞, and $F(k_0/k_\infty)$. It must be emphasized that this chapter is far from being closed. Our theoretical understanding of the required details is still fragmentary and at best semiquantitative. Nevertheless, the described procedure allows for a gradual implementation of improvements whenever these become available.

Because all microscopic steps are superimposed in the intermediate falloff range, it appears most reasonable to analyze the limiting ranges first where the contributing phenomena are separated to a major extent. One cannot expect to understand the full falloff curve when the simpler problems of understanding the limiting low- and high-pressure rate coefficients have not yet been solved. For this reason, the limiting ranges are considered separately in the following. A section on broadening factors then fol-

lows. Some short remarks on the few reactions, which possibly follow the radical complex mechanism, conclude this review.

2. High-Pressure Range

At high pressures, the association reaction is "capture-controlled": each encounter between A and B, which forms a long-lived AB*, leads to reaction because rapid collisional stabilization of AB* prevents redissociation and leads to stable AB. At this stage, we do not discuss what happens at very high pressures when the capture becomes diffusion-controlled. Instead, we consider a series of theoretical approaches which provide useful insight into the quantitative nature of k_∞ under normal gas-phase conditions.

First, suitable information about the potential energy surface (PES) of AB is required. Within the most simple approximation, one may consider a Morse potential in center-of-mass coordinates between A and B. At the same time, some model for the anisotropy of the potential has to be set up. Both components of the potential are important, the former characterizing centrifugal barriers $E_0(J)$, the latter describing the transformation of rotations of A and B into vibrational motions in AB which reduces the entropy of the collision pair. The Morse potential is expressed in the form

$$V(r) = -2D \exp[-\beta(r - r_e)] + D \exp[-2\beta(r - r_e)] \quad (14)$$

with the center-of-mass distance r between A and B, the Morse bond energy D, the equilibrium value r_e of r, and the Morse parameter β. Center-of-mass coordinates r in eq 14 are used for convenience because they allow for the simplest access to the centrifugal barriers $E_0(J)$. It should be emphasized, however, that the transition from bond lengths R, like those usually employed in Morse potentials, to center-of-mass coordinates r may also require changes in β.

We have proposed[12] to characterize the simplest kind of anisotropy in valence potentials by an r dependence of the quanta $\epsilon(r)$ of those bending vibrations which correlate with the rotations of A and B, e.g., in the form

$$\epsilon(r) \approx \epsilon(r_e) \exp[-\alpha(r - r_e)] \quad (15)$$

with a "looseness parameter" α. An analysis of experimental results for k_∞ in terms of a simplified statistical adiabatic channel model (SACM)[13] led to the suggestion that

$$\alpha/\beta \approx 0.5 \quad (16)$$

is a useful first approximation. In the meantime, a series of ab initio calculations of PESs have shown that reality is more complicated. Some potentials, such as those observed for some C−H or C−C bonds,[14] roughly follow eqs 14−16. On the other hand, systems with H−O, O−O, or N−O bonds often deviate markedly from this approximation. At long ranges, electrostatic potentials such as dipole−dipole or dipole−quadrupole potentials dominate and the transition to short-range valence potentials is not smooth, showing intermediate minima and maxima or shoulders of the PES.[15−19] Obviously, the electrostatic potentials differ from eqs 14−16. If ab initio calculations of the PES have not been carried out, eqs 14−16 may provide a useful starting point; if ab initio results are available, they have to be represented analytically and then allow for more accurate calculations such as those considered in the following.

It is not the aim of this review to discuss the large variety of possible PESs, although the capture rates and k_∞ directly depend on their properties. Instead, we show results for selected cases, illustrating possible absolute values and temperature dependences of k_∞. Our method of choice is a combination of classical trajectory calculations (CT) and the statistical adiabatic channel model (SACM).[12] The SACM treatment of "conserved modes" of A and B, changing their quanta only slightly during the capture process, provides a separation of these modes from the "transitional modes" which convert rotations of A and B into deformation vibrations of AB. The complicated capture dynamics of the transitional modes are best accessed by CT. It was shown[20] that the decoupling of conserved and transitional modes in calculating capture rates is justified. It was also shown[21,22] that the classical treatment of the transitional modes by CT is also fully adequate for all conditions of atmospheric interest (while quantum treatments are required for open-shell species in astrochemical applications).

Before explicitly calculating capture rate constants k_{cap}, one must consider the role of excited electronic states in the association process. Species A and B often are in open electronic shells such that several electronic states of AB* can be formed in the capture process. In general, most of these states cannot be collisionally quenched to form stable AB. One often even assumes that only the electronic ground state component of the formed states of AB* is relevant for the association reaction. In this case, k_∞ is given by

$$k_\infty = f_0 k_{cap} \quad (17)$$

where f_0 denotes the thermal population of those electronic configurations of A and B which form electronic ground state AB. f_0 generally is given by $Q_{el}(AB)/Q_{el}(A)Q_{el}(B)$, where Q_{el} terms are the respective electronic partition functions. f_0 can have a markedly negative dependence of T when electronic fine structure components of A and/or B are thermally populated like in HO radicals or O atoms.

The results of CT calculations for k_{cap} in the following are represented by two factors, the k_{cap}^{PST} value obtained by neglecting the anisotropy of the potential, which corresponds to "phase space theory" (PST), and a factor f_{rigid} describing the reduction of the rate constant by introduction of dynamical constraints arising from the anisotropy of the potential which is called the "rigidity factor". k_{cap}^{PST} can be calculated by CT. However, it can also be obtained by statistical rate theory from the centrifugal barriers

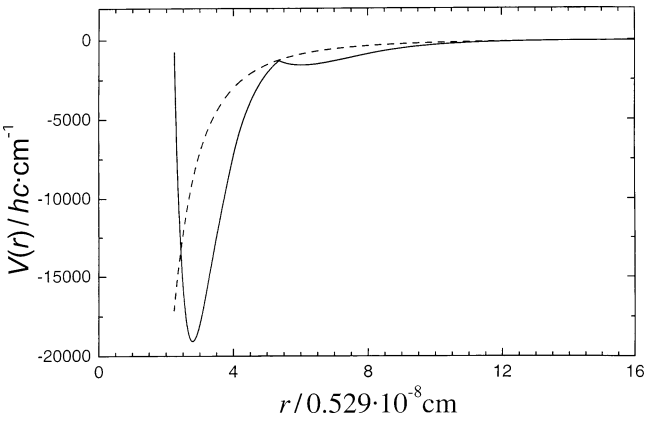

Figure 5. Minimum energy path potential for the HO + HO → H_2O_2 association reaction: (—) ab initio calculations from refs 15 and 16, with the outer potential well corresponding to HOHO and the inner well to HOOH, and (– – –) dipole–dipole potential[24].

$E_0(J)$ of the potential through

$$k_{cap}^{PST} = \frac{kT}{h}\left(\frac{h^2}{2\pi\mu kT}\right)^{3/2} Q_{cent}^{*} \qquad (18)$$

with the centrifugal partition function

$$Q_{cent}^{*} = \sum_{J=0}^{\infty}(2J+1)\exp[-E_0(J)/kT] \qquad (19)$$

and the reduced mass μ of the collision pair (A + B). k_{cap}^{PST} is determined by the true interaction potential between A and B through $E_0(J)$ to the extent that this is known. Otherwise, it appears more reasonable to employ an estimated Morse potential than to use a hypothetical van der Waals potential between A and B, as is sometimes done for simplification. It should be mentioned that eqs 18 and 19, with an ion-induced dipole potential, directly give the Langevin rate constant of ion-induced dipole capture which thus is a special case of PST.[23] For an isotropic potential, eqs 18 and 19 from statistical rate theory and CT determinations of k_{cap} give identical results.[21,22]

The centrifugal barriers $E_0(J)$ are important quantities in the analysis of k_∞, as well as of k_0 and $F(k_0/k_\infty)$, such that it is worthwhile to analyze their properties. For Morse-type potentials like eq 14, they are often of the form

$$E_0(J) \approx C_\nu[J(J+1)]^\nu \qquad (20)$$

with an exponent ν being between 1.0 and 1.5.[11] In this case

$$Q_{cent}^{*} \approx \Gamma(1+1/\nu)(kT/C_\nu)^{1/\nu} \qquad (21)$$

provides a direct access to the temperature dependence of k_{cap}^{PST}. The situation changes for more complicated potentials. We use the association reaction

$$HO + HO\ (+M) \rightarrow H_2O_2\ (+M) \qquad (22)$$

as an example. The ab initio calculations[15,16] have given a potential $V(r)$, as illustrated in Figure 5. The long-range dipole–dipole attraction leads to an HOHO structure which via an intermediate maximum, a potential "reef", finally is converted into the short-range valence structure of HOOH. The corresponding centrifugal barriers[24] are shown in Figure 6. Generally, the centrifugal barriers for different J values are found at different values of the distance r. However, in this special case, they are fixed for a certain range of J values at the position of the small intermediate reef of the potential.

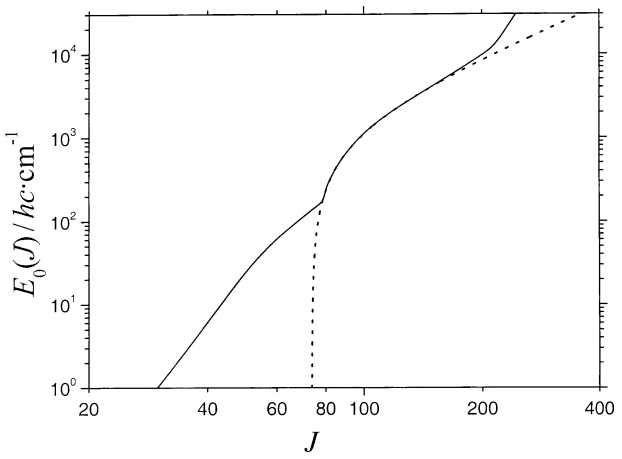

Figure 6. Centrifugal barriers $E_0(J)$ for the HO + HO → H_2O_2 association reaction: $J < 70$, as for dipole–dipole potential, (- - -) as for potential "reef"; and $J > 300$, as for H_2O_2 valence potential (see the text; results from ref 24).

Once the anisotropy of the potential in the form of eq 15 has been introduced, systematic CT calculations have been performed[21,22] for a variety of association processes such as atoms combining with linear molecules forming linear or T-shaped adducts, and linear species combining with linear species to form linear, T-shaped, or trapezoidal adducts. The resulting thermal rigidity factors $f_{rigid}(T)$, except at very high temperatures, were found to be practically independent of temperature. Their absolute value was found to be governed by "anisotropy parameters" of the type

$$C = [\epsilon(r_e)]^2/2B_\infty D \qquad (23)$$

with the adduct quanta $\epsilon(r_e)$ of the transitional modes (see eq 15), the rotational constants B_∞ of the corresponding rotations of the combining species A or B, and the Morse dissociation energy D. Depending on the number of deformation vibrations of the adduct correlating with the rotors of A or B, i.e., the number of transitional modes, the thermal rigidity factors could be expressed in terms of the parameters C; e.g., f_{rigid} was found to approach $\sqrt{(6/C)}$ for atomic A and linear B combining to form T-shaped AB, $\sqrt{2/C}$ for linear AB, or $2/C^2$ for linear A and linear B combining to form linear AB. With ν being in the range of 1.0–1.5 and α/β approximating 0.5, apart from a possible temperature dependence of the electronic partition functions $Q_{el}(A)$ and $Q_{el}(B)$ contained in f_0 in eq 17, this simple potential model then leads to an only very weak temperature dependence ($k_\infty \propto T^{0\pm0.5}$) of the high-pressure association rate constant. The influence of deviations of the ratio α/β from the "standard

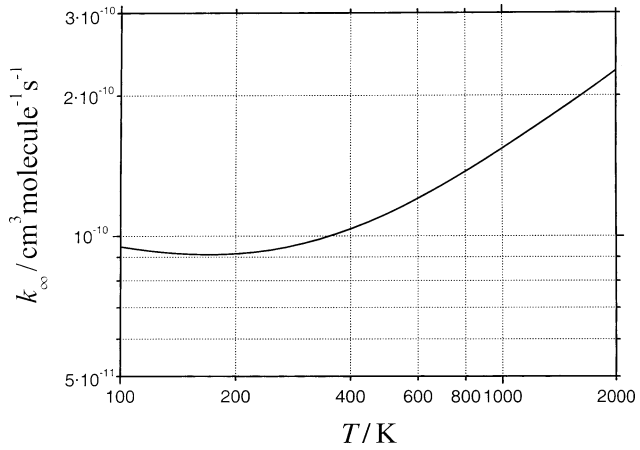

Figure 7. Limiting high-pressure rate constants k_∞ for the $H + O_2 \rightarrow HO_2$ association reaction (SACM/CT calculations on the ab initio potential from ref 17).

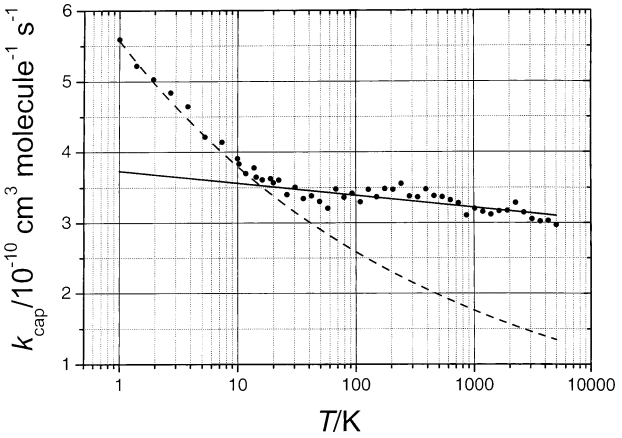

Figure 8. Capture rate constants k_{cap} (i.e., k_∞ omitting electronic weight factor f_0 in eq 17) for the $HO + HO \rightarrow H_2O_2$ association reaction: (●) SACM/CT calculations on the ab initio potential from ref 24, (– – –) dipole–dipole capture, and (—) fit to high-temperature results.

value" of 0.5 on $f_{rigid}(T)$ has also been inspected:[22] α/β values of <0.5 lead to slightly positive and α/β values of >0.5 to slightly negative temperature coefficients of f_{rigid}. However, these effects all are only weak and do not change the conclusions about an only weak T dependence of k_∞.

Before these results are compared with CT calculations on ab initio PESs, an inspection of association rate constants for electrostatic potentials appears to be illustrative: the association of ions with induced dipoles is characterized by an f_{rigid} of 1 and a temperature-independent k_∞ like that given by the Langevin rate constant; the association of ions with permanent dipoles leads to an f_{rigid} of 0.5 and a k_∞ that proportional to $T^{-0.5}$ such as given by locked-dipole capture theory;[25] the association of two dipoles leads to an f_{rigid} of 0.354[26] and a k_∞ that is proportional to $T^{-1/6}$. All these results suggest that, apart from the electronic factor f_0 in eq 14, k_∞ will have an only very weak temperature dependence.

Ab initio results so far are only available for few systems with three- and four-atom adducts AB such as the $H + O_2 \rightarrow HO_2$,[17] $HO + O \rightarrow HO_2$,[18] $O + NO \rightarrow NO_2$,[19] and $2HO \rightarrow H_2O_2$ association reactions.[24] Figure 7 shows calculated k_∞ results for the $H + O_2 \rightarrow HO_2$ reaction, while Figure 8 demonstrates the H_2O_2 system. The temperature dependences of k_{cap} are only weak and practically negligible over the atmospheric temperature range. Most of the predicted temperature dependence in the H_2O_2 system (not shown in Figure 8!) stems from the electronic factor f_0 with the well-known electronic partition functions of OH radicals. The rigidity factor of 0.35 near 300 K for the HO_2 system is close to the value estimated with a C of ≈22 from eq 23 for a nonlinear adduct, being between a linear and T-shaped structure.[17] The results for the H_2O_2 system show that k_{cap} is governed by the dipole–dipole potential only up to temperatures near 30 K. Under atmospheric conditions, the intermediate potential maximum (being nevertheless at energies of <0) dominates k_∞. The rigidity factor here is still close to 0.35, i.e., to that of the dipole–dipole potential, but the centrifugal barriers correspond to a fixed position of an effective activated complex. This in turn corresponds to a ν of 1 in eq 20 and, through eqs 18–21 to a k_{cap} that is proportional to $T^{0.5}$. The weak negative temperature coefficient of f_0 in k_∞ then largely compensates for this temperature dependence.

Following the SACM/CT approach, k_∞ only includes contributions from the transitional modes. One, therefore, should not expect changes in the situation that is described when larger polyatomic species A and B are considered for which ab initio calculations of the potential are not available. The assumption of a nearly temperature independent k_{cap} and of an only weak temperature dependence of k_∞ from the electronic factor f_0, therefore, appears to be safe in all cases. Small true activation barriers of the potential (being positive), however, certainly change the picture. In this case, the treatment of rigid activated complex RRKM theory should be approached, leading to positive temperature coefficients and smaller values of k_∞. Whenever experimental studies of association reactions seem to indicate that k_∞ has a strong negative temperature coefficient, one has to suspect that the evaluation is inadequate because the pressure range of the experiments was too small to allow for a meaningful extrapolation toward k_∞.

It is well-known that dynamical and statistical calculations of k_∞ are equivalent if the same phase space distributions are accurately realized.[27] For this reason, the SACM/CT approach may be approximated by variational transition state theory (VTST) and its variants such as those used in VARIFLEX codes[28] of flexible transition state theory.[29,30] In any case, however, the quality of the results is primarily governed by the quality of the employed potential. We feel that the SACM/CT treatment is particularly direct, rationalizes the contributions of the minimum energy path leading to the centrifugal barriers (in k_{cap}^{PST}) and of the anisotropy introducing additional dynamical constraints (in f_{rigid}), and does not need corrections for quantitation and recrossing trajectories as this is the case with VTST. In most practical cases, when ab initio potentials are not available, experimental conclusions about k_∞ in comparison to theoretical considerations provide the most reliable information anyway.

Table 1. Rate Parameters for Atmospheric Association Reactions[a]

reaction	$k_0/[N_2]$	n	k_∞	F_{center}
$H + O_2 \rightarrow HO_2$	5.4×10^{-32}	1.8	7.5×10^{-11}	0.55
$HO + HO \rightarrow H_2O_2$	6.9×10^{-31}	0.8	2.6×10^{-11}	0.5
$O + NO \rightarrow NO_2$	1.0×10^{-31}	1.6	3.0×10^{-11}	0.85
$HO + NO_2 \rightarrow HONO_2$	3.7×10^{-30}	2.9	3.6×10^{-11}	0.41
$NO_2 + NO_3 \rightarrow N_2O_5$	2.8×10^{-30}	3.5	2.0×10^{-12}	0.45
$ClO + NO_2 \rightarrow ClONO_2$	1.6×10^{-31}	3.4	1.5×10^{-11}	0.5
$BrO + NO_2 \rightarrow BrONO_2$	4.7×10^{-31}	3.1	1.4×10^{-11}	0.4
$IO + NO_2 \rightarrow IONO_2$	7.7×10^{-31}	5.0	1.6×10^{-11}	0.4
$HO + C_2H_4 \rightarrow HOC_2H_4$	7.0×10^{-29}	3.1	9.0×10^{-12}	0.48
$HO + C_3H_6 \rightarrow HOC_3H_6$	8.0×10^{-27}	3.5	3.0×10^{-11}	0.5
$O_2 + CH_3 \rightarrow CH_3O_2$	1.0×10^{-30}	3.3	1.8×10^{-12}	0.27
$CH_3O_2 + NO_2 \rightarrow CH_3O_2NO_2$	2.5×10^{-30}	5.5	7.5×10^{-11}	0.36
$C_2H_5O_2 + NO_2 \rightarrow C_2H_5O_2NO_2$	1.3×10^{-29}	6.2	8.8×10^{-12}	0.31
$CH_3CO_3 + NO_2 \rightarrow CH_3CO_3NO_2$	2.7×10^{-28}	7.1	1.2×10^{-11}	0.30

[a] Selected values from the IUPAC data evaluation:[1] $k_0/[N_2]$ in cm^6 molecule^{-2} s^{-1}, k_∞ in cm^3 molecule^{-1} s^{-1}, values for 300 K, $k_0 \propto T^{-n}$, $k_\infty \propto T^m$ with $m \approx 0$, falloff curves with eqs 35 and 36 and temperature-independent F_{center}.

Representing k_{cap} by the "hindered Gorin model",[31] one identifies the unhindered Gorin rate constant with PST and the thermal rigidity factor f_{rigid} with $1 - \eta$, where η is an empirical "hindrance parameter". The relation between f_{rigid} and the anisotropy of the potential, as described above, therefore can also be used to characterize η.

A selection of experimentally derived values of k_∞ in Table 1 for illustration are reproduced from data evaluations such as ref *1*. These results show which variations of k_∞ must be expected. With regard to the accuracy of the given values, one should keep in mind that the values all are from extrapolations which to some extent rely on the chosen broadening factors $F(k_0/k_\infty)$ of the falloff curves and also on the chosen low-pressure rate constants k_0. This uncertainty becomes larger as smaller AB adducts are considered.

3. Low-Pressure Range

The analysis of high-pressure rate coefficients in the previous section dealt with "activated complex properties", as hidden and implicit as they may have been in our treatment. Low-pressure rate coefficients, in contrast to this, are governed by intermolecular collisional energy transfer between AB* and M. However, some properties of the potential energy surface such as the centrifugal barriers $E_0(J)$ also enter the rate coefficients to a limited extent. In the low-pressure limit, a A + B $\Leftrightarrow$ AB* pre-equilibrium is established, and the effective rate of collisional stabilization of AB* determines the overall rate of formation of AB. Obviously, the populations of states $g(E)$ of AB* then deviate from equilibrium populations $f(E)$. A similar situation prevails in the low-pressure range of the reverse thermal dissociation reactions. It appears worthwhile to remember that, at steady state, the nonequilibrium factors $[h(E) = g(E)/f(E)]$ of dissociation and association are complementary[32]

$$h_{diss}(E) + h_{ass}(E) = 1 \tag{24}$$

Likewise, the overall rate coefficients of dissociation and association, at steady state, despite quite different nonequilibrium populations of the states of AB*, are coupled by the equilibrium constant K_{eq}

$$k_{ass} = k_{diss} K_{eq} \tag{25}$$

The determination of k_0 requires the solution of a master equation leading to the steady-state populations $g(E,J)$ and from this to the rate coefficient k_0. The input for this treatment are state (E,J)-to-state (E',J') collisional energy transfer rates which may be separated into an overall collision frequency Z and state-to-state transition probabilities $P(E',J'/E,J)$. It appears strange that classical unimolecular rate theory in the RRKM version has assumed strong collisions, thus drawing attention away from the rate-determining process to the more "trivial" statistical factors. However, the solution of the master equation, particularly under steady-state conditions, today has become routine. It is known[32] that most of the details of energy transfer are lost by thermal averaging and that only Z, $\langle\Delta E\rangle$, and $\langle\Delta E^2\rangle$ enter k_0, where $\langle\Delta E\rangle$ and $\langle\Delta E^2\rangle$ are the first and second moments of $P(E',J'/E,J)$, respectively, i.e., the average and average squared step sizes of energy transfer, respectively. Experimental determinations of $\langle\Delta E\rangle$ and $\langle\Delta E^2\rangle$ are now available for selected systems; see, for example, ref 33. However, rotational effects are still badly characterized such that solutions of the two-dimensional (E,J) master equation remain to be introduced in the future. Solving the master equation is not the problem, but having realistic input parameters for the energy transfer process is.

The solution of the master equation in the low-pressure range can be expressed by

$$k_0 = K_{eq}\beta_c Z[M]\sum_{J=0}^{\infty}(2J+1)\int_{E_0(J)}^{\infty} dE f(E,J) \tag{26}$$

where, for an exponential collision model of $P(E'/E)$, the collision efficiency β_c is related to $\langle\Delta E\rangle$ by[32]

$$\beta_c/(1 - \sqrt{\beta_c}) \approx -\langle\Delta E\rangle/F_E kT \tag{27}$$

with

$$F_E = \int_{E_0}^{\infty} f(E)\, dE/f(E_0)kT \tag{28}$$

Provided that the equilibrium populations $f(E,J)$ and the centrifugal barriers $E_0(J)$ are known, the treatment can concentrate on essential factors Z and $\langle\Delta E\rangle$. An economic way to represent the factors included in $f(E,J)$ was proposed,[11,32] giving

$$k_0 = \beta_c Z[\mathrm{M}]\rho_{\mathrm{vib,h}}(E_0)F_E kTF_{\mathrm{anh}}F_{\mathrm{rot}} \times \frac{Q_{\mathrm{el,rot}}(\mathrm{AB})\exp(-E_0/kT)}{Q_{\mathrm{el,rot}}(\mathrm{A})Q_{\mathrm{el,rot}}(\mathrm{B})Q_{\mathrm{vib}}(\mathrm{A})Q_{\mathrm{vib}}(\mathrm{B})} \quad (29)$$

The threshold energy [$E_0 = E_0(J=0)$] here is counted from the energy of separated A and B, i.e., barrierless associations have E_0 values of 0. Q terms denote the relevant partition functions, and internal rotations are included in the vibrational partition functions. The rotational factor F_{rot} includes centrifugal contributions through $E_0(J)$; for details, see ref 11. While the calculation of vibrational harmonic densities of states $\rho_{\mathrm{vib,h}}(E_0)$, as well as of the rotational factor F_{rot} [once $E_0(J)$ is known], is trivial,[11,32] the problem of properly handling the anharmonicity factor F_{anh} essentially remains unsolved. First propositions,[32] which were based on the anharmonicities of Morse potentials, apparently underestimate F_{anh}. Simplified methods for including stretch−bend couplings[34] seem to work well[35] but need to be validated for larger molecules. When the various contributions to k_0 are considered, there remain some uncertainties in F_{rot} [through uncertainties in the potential and, hence, in $E_0(J)$], in F_{anh} (mainly through uncertainties in stretch−bend couplings), and in collision parameters Z and β_c. For the latter, the following situation prevails: The collision frequencies Z apparently can be represented by capture rate constants between AB* and M. If there is no particularly pronounced interaction, the Lennard-Jones collision frequency Z_{LJ} appears to be an adequate choice for Z.[32] If long-range forces operate, such as with an M of H_2O,[36] the corresponding capture rate constant represents Z; likewise, if M is a reactive atom,[37] the corresponding capture rate constant, as analyzed in section 2, represents Z (by analogy Z is equal to the Langevin rate constant, if AB is an ion and if M is an induced dipole). $\langle\Delta E\rangle$ values still have to be taken as fit parameters. However, by comparison of experimental results for groups of reactions, certain general rules could be derived. As far as atmospheric association reactions are concerned, the most relevant are the assumptions of a temperature independent $\langle\Delta E\rangle$ of $Z = Z_{\mathrm{LJ}}$ (except for conditions under which $[H_2O]/[N_2 + O_2] > 0.03$), and of $\langle\Delta E\rangle/hc \approx -200 \pm 100\ \mathrm{cm}^{-1}$ for N_2 or O_2 as M. CT determinations of Z and $\langle\Delta E\rangle$ are also making progress and will become useful for quantitative predictions in the future.

Despite the mentioned uncertainties in the various factors contributing to k_0, a theoretical analysis of experimental results in terms of eq 29 should always be made to trace experimental misinterpretations. There is only little uncertainty in the predicted temperature dependence of k_0. Also, absolute values of k_0 can probably be predicted from eq 29 with an uncertainty of less than a factor of 3. However, whenever the results of the theoretical analysis are reported, all of the used details should be indicated, in particular $E_0(J)$, F_{anh}, $\langle\Delta E\rangle$, and Z. Ready-to-use codes that do not specify the underlying assumptions and parameters become intransparent and, hence, are only of limited value.

In contrast to the generally only weak temperature dependence of k_∞, k_0 may have strongly negative temperature coefficients

$$k_0 \propto T^{-n} \quad (30)$$

The exponent n will be the larger as there are more oscillators in AB and the lower are their frequencies. At the same time, the absolute value of k_0 increases to such an extent that the low-pressure range becomes more and more difficult to reach with decreasing pressure. Figures 1−3 demonstrate this shift of the falloff curves with pressure. The main culprit for this effect is the vibrational density of states $\rho_{\mathrm{vib,h}}(E_0)$ in eq 29 which dramatically increases with an increase in the number of oscillators and a decrease in oscillator frequencies. For illustration, Table 1 includes experimental values of k_0 for some atmospheric association reactions like those evaluated in ref 1. Exponents n from eq 30 are also given.

4. Falloff Range

The analysis of the rate coefficients k in the intermediate falloff range presents an interesting situation. On one hand, the difficulties of a separate understanding of k_0 or k_∞ have not been overcome so that the by far more complicated general analysis of the falloff range seems out of reach. Once k_0 and k_∞ have been determined by a combination of experiment and theory, on the other hand, reduced falloff curves can be constructed with sufficient reliability even by suitably simplified theoretical models. This allows for an often satisfactory solution of the practical problem of properly representing k. In this section, some new results for representing k/k_∞ as a function of k_0/k_∞ are described. One first notices that, according to eq 25, reduced falloff curves of this type are identical for association and the reverse dissociation processes. The broadening factors $F(k_0/k_\infty)$, then, may be factorized into strong-collision and weak-collision contributions through

$$F(k_0/k_\infty) = F^{\mathrm{SC}}(k_0/k_\infty)F^{\mathrm{WC}}(k_0/k_\infty) \quad (31)$$

The strong-collision broadening factor $F^{\mathrm{SC}}(k_0/k_\infty)$ can be derived from the expression for k in standard unimolecular rate theory. For convenience, we use that for the dissociation rate constant k_{diss}

$$k_{\mathrm{diss}} = \sum_{J=0}^{\infty}(2J+1)\int_{E_0(J)}^{\infty} \mathrm{d}E \frac{k(E,J)f(E,J)Z[\mathrm{M}]}{k(E,J) + Z[\mathrm{M}]} \quad (32)$$

where, in eq 4, k_{-1} corresponds to $k(E,J)$ and k_1 to $k(E,J)f(E,J)K_{\mathrm{eq}}$. The specific rate constants for dissociation $k(E,J)$ in statistical unimolecular rate theory are expressed by

$$k(E,J) = W(E,J)/h\rho(E,J) \quad (33)$$

with the number of open dissociation channels $W(E,J)$

and the rovibrational density of states $\rho(E,J)$ of AB. The thermal average over $W(E,J)$ leads to k_∞. An explicit specification of the E and J dependences of $W(E,J)$ and $\rho(E,J)$ is required for the falloff range.

Reduced falloff curves first were expressed in terms of Kassel integrals with the parameters S_K ($\approx E_{vib}/kT$) and B_K ($\approx E_0/kT$).[39] Later on, rigid activated complex RRKM theory was exploited[11,39] to obtain theoretical expressions for $F^{SC}(k_0/k_\infty)$. In this approach, J dependences in eq 32 were neglected and the results were represented in the form of eq 12. Bell-shaped expressions similar to Figure 4 were obtained in this way which conveniently could be approximated by

$$F^{SC}(k_0/k_\infty) \approx F_{center}^{SC\{1+[\log(k_0/k_\infty)/N]^2\}^{-1}} \quad (34)$$

The width parameter N was found to be coupled to F_{center}^{SC} through

$$N \approx 0.75 - 1.27 \log F_{center}^{SC} \quad (35)$$

With an increasing extent of broadening, asymmetries of the bell-shaped functions of $F^{SC}(k_0/k_\infty)$ were also observed[39] which we do not consider here.

In addition to the shape of the broadening factors, such as approximated by eqs 34 and 35, the analysis of falloff curves from RRKM theory provided expressions for the center broadening factors F_{center}^{SC}. It was shown[11,39] that F_{center}^{SC} can be expressed conveniently in terms of modifications of the Kassel parameters S_K and B_K such that the absolute values and temperature dependences of F_{center}^{SC} are accessible from theory.

Collisional energy transfer of weak collision type also has some influence on the shape of the reduced falloff curves. These effects cannot simply be ascribed to replacement of Z in eq 32 with $\beta_c Z$ which would not change the broadening factors. Instead, weak collisions generally tend to further broaden the reduced falloff curves; i.e., $F^{WC}(k_0/k_\infty) < 1$ in eq 31. To determine $F^{WC}(k_0/k_\infty)$, the complete master equation for dissociation, association, activating, and deactivating collisions has to be solved. Examples of such calculations have been described previously.[40,41] As a general result, $F^{WC}(k_0/k_\infty)$ was found to be similar in shape to $F^{SC}(k_0/k_\infty)$, however, with a weak collision center broadening factor depending on $\langle\Delta E\rangle$. To a first approximation, an expression of the type[40]

$$\log F_{center}^{WC} \approx 0.14 \log \beta_c \quad (36)$$

was found to apply. Using a combined F_{center}, eqs 34 and 35 then are used (omitting the superscript SC) for the combined effects of weak and strong collision broadening.

In practice, the following procedures have become customary. The NASA/JPL evaluation of atmospheric reactions[2] used eqs 34 and 35 with an F_{center} of $\approx$0.6 and an N of $\approx$1.0 independent of the system and temperature. In contrast to this, the IUPAC evaluation[1] employed eqs 34 and 35 with a system-dependent F_{center}. Often, F_{center} is also being used as an empirical fit parameter of the experimental data. It cannot be sufficiently emphasized that the derived expressions for k_0, k_∞, and F_{center} have to be considered together, because the extrapolated values of k_0 and k_∞ often depend on the chosen value of F_{center} [as well as on the chosen expression for $F(k_0/k_\infty)$, using $N = 1$ or N from eq 35]; see below.

It may appear to be unsatisfactory that the NASA/JPL and IUPAC evaluations used different policies for the representation of falloff curves through different values of F_{center}. In practice, however, there are only small differences in the results as long as only limited parts of the falloff curves are represented and if the procedure is clearly defined by specifying the used k_0, k_∞, and F_{center}. For a further more quantitative comparison of experiment and theory, however, it should be recognized that the NASA/JPL policy might have to be modified because F_{center} clearly must be system-dependent and the values for k_0 and k_∞ extracted on the basis of a constant F_{center} of 0.6 cannot be absolutely correct. This, however, requires more certainty about the adequate F_{cent} which has to come from theory. A number of attempts in this direction have been made. First, it was realized that eqs 34 and 35 may not be the best way to represent reduced falloff curves from RRKM theory. Asymmetries were introduced,[11,39,40] and different functional forms were recommended.[41−44] These approaches, however, do not appear to improve the situation since rigid activated complex RRKM theory does not apply to the considered barrierless association reactions anyway. They may appear to apply to reactions with small barriers, but even here, rotational effects have not been included and weak collision effects were not adequately accounted for. In practice, often numerical master equation/flexible transition state codes are employed. If these results are represented in a way which indicates k_0, k_∞, and F_{center}, they provide valuable information about F_{center}. However, this approach will become really meaningful only when $k(E,J)$ is included as it is derived from ab initio potentials, when sufficient information about rovibrational collisional energy transfer is available, and when two-dimensional (E,J) master equations are employed. Since these requirements cannot be fulfilled at present, we do not review this line of developments. Instead, I feel that, at this stage, one has to be content with simpler procedures. (i) Equations 34 and 35 may serve as a starting point to be improved only when more detailed calculations require modifications. (ii) Equation 36 may provide a first guess for weak collision broadening to be improved when reliable information about β_c and $\langle\Delta E\rangle$ is available. (iii) F_{center}^{SC} should be changed from the expressions based on rigid activated complex RRKM theory which are not appropriate for barrierless association reactions. Since this last point is very important and was the subject of recent activities,[45−48] in the following we summarize the corresponding results.

For low temperatures such as those relevant to atmospheric applications, most (if not all) of the oscillators of A and B are of such large frequencies that they do not contribute to the Kassel parameter S_K. In early unimolecular reaction studies, this

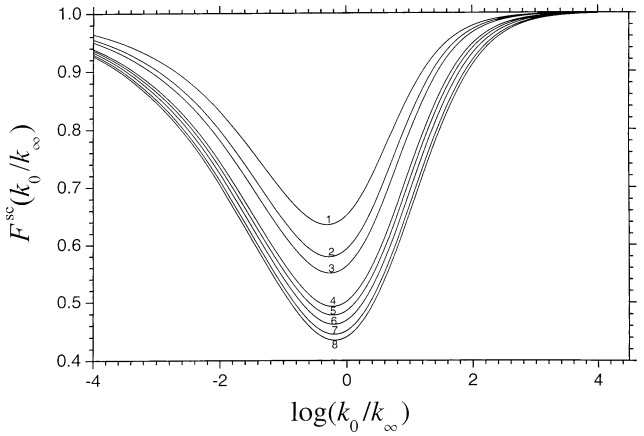

Figure 9. Strong collision broadening factors $F^{SC}(k_0/k_\infty)$ for the HO + NO_2 (+M) → $HONO_2$ (+M) association reaction. Results from ref 46 for T/K values of 1400 (curve 1), 1000 (curve 2), 800 (curve 3), 400 (curve 4), 300 (curve 5), 200 (curve 6), 100 (curve 7), and 50 (curve 8).

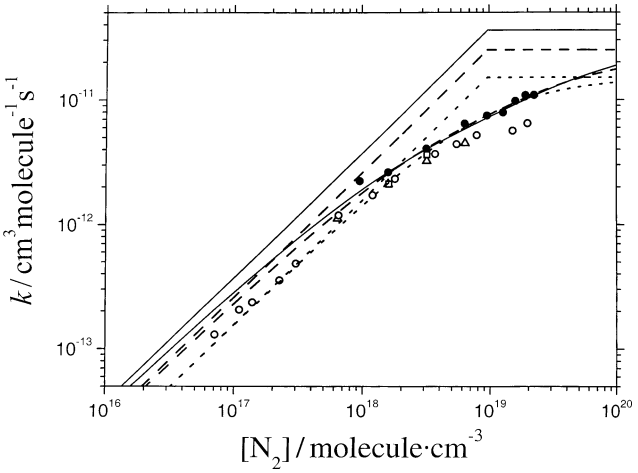

Figure 10. Falloff curves for the HO + NO_2 (+N_2) → $HONO_2$ (+N_2) association reaction. Experiments at 296 K from refs 52 (□), 54 (●), 55 (○), and 56 (△). Fit to the results from ref 55 by eqs 34 and 35 with an F_{center} of 1, a k_0 of $1.56 \times 10^{-30} \times [N_2]$, and a k_∞ of 1.5×10^{-11} (- - -), with an F_{center} of 0.6, a k_0 of $2.58 \times 10^{-30} \times [N_2]$, and a k_∞ of 2.5×10^{-11} (— — —), and with an F_{center} of 0.4, a k_0 of $3.7 \times 10^{-30} \times [N_2]$ cm^6 molecule^{-2} s^{-1}, and a k_∞ of 3.6×10^{-11} cm^3 molecule^{-1} s^{-1} (—), in agreement with the experimental k_∞ when M is He from ref 57.

erroneously was interpreted as an indication for restricted intramolecular energy flow in AB*, while in reality, it is a pure quantum effect in the statistics. In contrast to the conserved oscillators, the transitional modes approach rotational character and thus classically contribute to the effective S_K. However, these modes couple with orbital rotation and are restricted by centrifugal barriers and anisotropy constraints. For this reason, rotational effects of the falloff curves, like those included in eq 32, have to be elucidated in detail. This can be done in two stages: first by determining $k(E,J)$ from phase space theory which can be done without great effort,[49,50] although the centrifugal barriers $E_0(J)$ need to be known, and second by determining (E,J)-specific rigidity factors $f_{rigid}(E,J)$ by SACM/CT calculations.[51] It turns out that the PST treatment gives the major contribution to $F^{SC}(k_0/k_\infty)$. We use the formation of nitric acid from the association of HO with NO_2[46] as an illustrative example; see Figure 9. One obtains an F^{SC}_{center} of ≈0.47 over the range of 200−400 K. Together, with an additional weak collision broadening described by eq 36, one derives an F_{center} of ≈0.40 ± 0.02 which is in good agreement with a fitted experimental value for F_{center} of ≈0.44 when M is N_2 at 300 K.[52−56] Obviously, the NASA/JPL value of 0.6 is too high and, if used for a fit, leads to k_0 and/or k_∞ values which are too low by a factor of up to 1.5. It was found[46] that the PST calculation of $F^{SC}(k_0/k_\infty)$ nearly produced the final result and that the introduction of the somewhat uncertain rigidity factors, depending on fine details of the potential, had practically no effect. Therefore, on the basis of the centrifugal barriers which have to be known for an analysis of k_0 and k_∞ anyway, and using PST, reduced falloff curves can be calculated relatively easily, as demonstrated in ref 46. At this stage, we have assumed that the reaction only occurs on one channel; i.e., the possible contribution from a second channel, HO + NO_2 → HOONO, was not taken into account (see below). A temperature dependence of F_{center} can practically be neglected for atmospheric applications. While the bell-shaped form of $F(k_0/k_\infty)$ in Figure 9 is roughly conserved, one nevertheless notices minor asymmetries. Also, the k_0/k_∞ minimum is slightly shifted from 1 to smaller values. One may account for this in the way described in ref 39 or in some other empirical way. However, eqs 34 and 35 appear to be sufficient within experimental uncertainties. Nevertheless, future improvement will become necessary when the experimental precision increases. One should also not forget that at higher temperatures conserved oscillators will also start to contribute to S_K which leads to a further decrease in F^{SC}_{center}, as has been systematically documented in refs 39 and 45.

Before leaving the discussion of falloff curves, we briefly demonstrate the consequences of choosing different values of F_{center}. Figure 10 shows fits of falloff curves with F_{center} values of 1, 0.6, and 0.4 to experimental data for the HO + NO_2 (+N_2) → HNO_3 (+N_2) association reaction. Different values of k_0 and k_∞ are derived, depending on the choice of F_{center}. The scatter of the experimental results does not allow us to make a definite decision on the value of F_{center} (although an F_{center} of 1 can be excluded with certainty). For this reason, the main advantage of using a realistic F_{center} from theory lies in the possibility of extrapolating experimental parts of the falloff curve to realistic values of k_0 and k_∞ which is not case when unrealistic values of F_{center} are used. Figure 10 also demonstrates experimental uncertainties which are not understood at present. In view of the importance of the considered reaction, the remaining uncertainty appears to be most unfortunate and calls for improved experiments.

The HNO_3 system may be even more complicated for another reason. When HO radicals combine with NO_2, there is the possibility of forming various HNO_3 isomers such as ordinary nitric acid $HONO_2$ or HOONO. In this case, to a first approximation, the overall rate may be split into the sum of the rates

for the various channels. This may influence the shape of the overall falloff curve which would be difficult to identify. More conclusive are isotopic studies or experiments showing nonexponential concentration−time profiles of HO radicals due to redissociation of the less stable isomers. For a discussion of this topic, see refs 53−57.

The approach illustrated for the HNO_3 system in ref 48 has been generalized to molecules with similar energy and frequency parameters but with different total numbers r of rotational degrees of freedom of A and B. The derived values of $F_{\text{center}}^{\text{SC}}$, together with an $F_{\text{center}}^{\text{WC}}$ of ≈0.85, gave total values of F_{center} which may serve for a quick estimate. F_{center} values of ≈0.53, ≈0.50, ≈0.45, ≈0.40, and ≈0.35 were obtained[48] in this way for r values of 2−6, respectively (for more details, see ref 48).

5. Radical Complex Mechanism

The $O + O_2 + M \rightarrow O_3 + M$,[58] $Cl + O_2 + M \rightarrow ClOO + M$,[59] and $ClO + ClO + M \rightarrow Cl_2O_2 + M$[60] association reactions have shown a series of "anomalies". The low pressure rate coefficients were found to be markedly larger than values that can be explained by eq 29. They had much stronger dependences on the nature of M. They had temperature dependences stronger than those predicted by this equation. In addition, for the O_3 and Cl_2O_2 systems, unusual pressure dependences, significantly differing from typical falloff curves, were observed at pressures above 1 bar. Figure 11 illustrates the unusual pressure dependence for the rate coefficient for ozone formation in the bath gas N_2. Obviously, the observed dependence of k on N_2 concentration markedly differs from the usual picture of falloff curves. Furthermore, Figure 12 shows unusual results for the temperature dependence of the low-pressure rate coefficient of ozone formation in the bath gases He, Ar, and N_2. It has been postulated[58−60] that these effects are due to a dominance of a radical complex mechanism (see eqs 5−7) over the usual energy transfer mechanism of eqs 1−4. This change of mechanism may occur when the density of states $\rho_{\text{vib,h}}(E_0)$ in eq 29 is so small that eq 7 exceeds eq 4. The radical complex mechanism

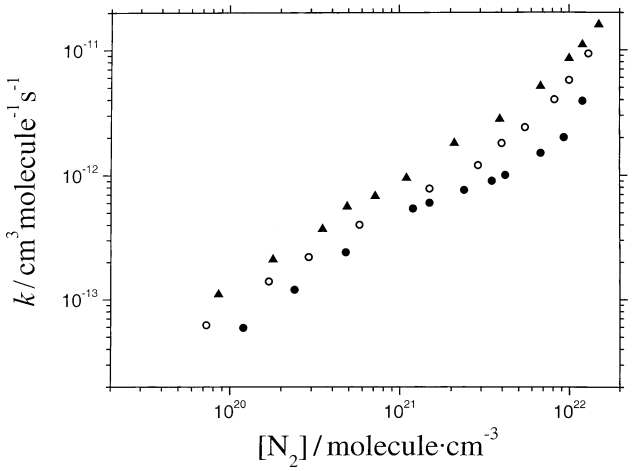

Figure 11. Rate coefficients for the $O + O_2$ (+N_2) → O_3 (+N_2) association reaction at 213 (▲), 253 (●), and 300 K (○) (measurements from ref 58, suggesting dominance of the radical complex mechanism; see the text).

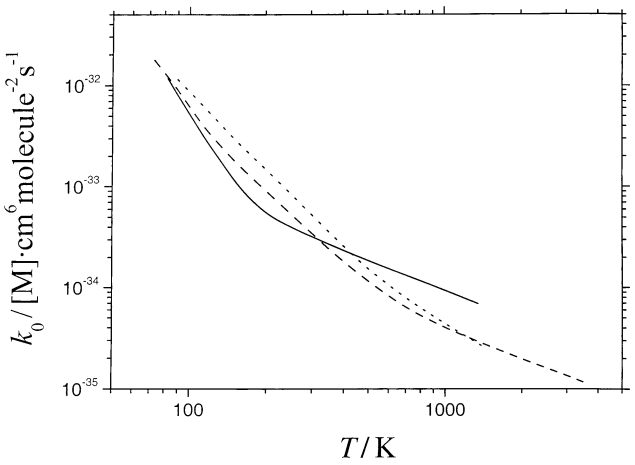

Figure 12. Low-pressure rate coefficients for the $O + O_2$ (+M) → O_3 (+M) association reaction when M is N_2, Ar, and He (from top to bottom at 300 K; measurements from various laboratories as summarized in ref 58, suggesting a transition from the radical complex mechanism at low T to the energy transfer mechanism at high T; see the text).

dominates the association of atoms with diatomic molecules. A few three- or four-atom systems with small values of the adduct dissociation energies E_0 apparently also follow this behavior. The value of K_5 and its temperature dependence are governed by the strength of the A−M bond in eq 5. The mechanism that is followed may, therefore, depend on the nature of the bath gas M and the temperature. The results from ref 58 indicate that the $O + O_2 + He \rightarrow O_3 + He$ reaction at temperatures up to 200 K follows the radical complex mechanism, while the association at >200 K and the reverse dissociation at 1000 K follow the energy transfer mechanism. Figure 12 indicates that the corresponding change in mechanism when M is Ar occurs near 500 K, while it occurs near 800 K when M is N_2. The observed pressure dependences, at pressures above 1 bar, are so unusual that larger complexes and higher excited electronic states may also be involved which require an extension of the treatment beyond eqs 5−7. We do not intend to analyze the radical complex mechanism at this place; for more details, see the discussion in ref 58. Instead, we only point out that these reactions stick out from the representations given in Table 1 for the reasons mentioned in this section.

6. Conclusions

The complicated dependence of the rates of association reactions, as they are frequently encountered in atmospheric chemistry, on the temperature, on the concentration, and on the chemical nature of the third-body gases can be rationalized well in terms of unimolecular rate theory. Far from being mastered by ab initio rate theory, these reactions can be represented by a combination of experimental and theoretical results which leads to economic rate expressions. Although these differ from a simple two-parameter form such as the Arrhenius-type expression for direct bimolecular reactions, five parameters generally suffice for a data representation. These are the absolute values and the temperature coefficients of the limiting low- and high-pressure rate coefficients

$$k_0 = k_0(300\ \mathrm{K})(T/300\ \mathrm{K})^{-n} \quad (37)$$

$$k_\infty = k_\infty(300\ \mathrm{K})(T/300\ \mathrm{K})^{-m} \quad (38)$$

and a practically temperature-independent center broadening factor

$$F_{\mathrm{center}} \approx F_{\mathrm{center}}(300\ \mathrm{K}) \quad (39)$$

F_{center} can be estimated relatively easily from theory as demonstrated in refs 46 and 48. To a first approximation, one may use[48] F_{center} values of 0.35 for nonlinear A and nonlinear B, 0.40 for linear A and nonlinear B, 0.45 for linear A and linear B, 0.50 for atomic A and nonlinear B, and 0.53 for atomic A and linear B.

Finally, one may generally assume that m is close to zero ($m = 0 \pm 0.5$). Reactions with small barriers E_a have additional Boltzmann factors $\exp(-E_a/kT)$ in eqs 37 and 38. Association reactions leading to more than one isomer of AB have to be split into rate expressions for each channel. Associations of three- or four-atom adducts with small dissociation energies may follow the radical complex instead of the energy transfer mechanism, which requires a different kind of theory, although the results for k_0 can also be represented by eq 37.

7. Acknowledgments

Lively discussions of this issue with many colleagues, technical help by A. I. Maergoiz and V. G. Ushakov, and financial support by the Deutsche Forschungsgemeinschaft (SFB 357 "Molekulare Mechanismen unimolekularer Prozesse") are gratefully acknowledged.

8. References

(1) Atkinson, R.; Baulch, D. L.; Cox, R. A.; Hampson, R. F.; Kerr, J. A.; Rossi, M. J.; Troe, J. *J. Phys. Chem. Ref. Data* **2000**, *29*, 167; **1999**, *28*, 191; **1997**, *26*, 1329; **1997**, *26*, 521; and earlier references. See also http://www.iupac-kinetic.ch.com. ac.uk/.
(2) Sander, S. P.; Friedl, R. R.; Golden, D. M.; Kurylo, M. J.; Huie, R. E.; Orkin, V. L.; Moortgat, G. K.; Ravishankara, A. R.; Kolb, C. E.; Molina, M. J.; Finlayson-Pitts, B. J. *JPL Publ.* **2003**, *02*-25 (see http://jpldataeval.jpl.nasa.gov/). Sander, S. P.; Friedl, R. R.; DeMore, W. B.; Golden, D. M.; Kurylo, M. J.; Hampson, R. F.; Huie, R. E.; Moortgat, G. K.; Ravishankara, A. R.; Kolb, C. E.; Molina, M. J. *JPL Publ.* **2000**, *00*-3. De More, W. B.; Sander, S. P.; Golden, D. M.; Hampson, R. F.; Kurylo, M. J.; Howard, C. J.; Ravishankara, A. R.; Kolb, C. E.; Molina, M. J. *JPL Publ.* **1997**, *97*-4; **1994**, *94*-26; and earlier references.
(3) Cobos, C. J.; Hippler, H.; Troe, J. *J. Phys. Chem.* **1985**, *89*, 342. Hahn, J.; Krasnoperov, L.; Luther, K.; Troe, J. 17th International Gas Kinetics Symposium, Essen, Germany, 2000.
(4) Kircher, C. C.; Margitan, J. J.; Sander, S. P. *J. Phys. Chem.* **1984**, *88*, 4370.
(5) Croce de Cobos, A. E.; Hippler, H.; Troe, J. *J. Phys. Chem.* **1984**, *88*, 5083.
(6) Smith, C. A.; Ravishankara, A. R.; Wine, P. A. *J. Phys. Chem.* **1985**, *89*, 1423.
(7) Burrows, J. P.; Tyndall, G. S.; Moortgat, G. K. *J. Phys. Chem.* **1985**, *89*, 4848.
(8) Orlando, J. J.; Tyndall, G. S.; Cantrell, C. A.; Calvert, J. G. *J. Chem. Soc., Faraday Trans.* **1991**, *87*, 2345.
(9) Zellner, R.; Lorenz, K. *J. Phys. Chem.* **1984**, *88*, 984.
(10) Klein, Th.; Barnes, I.; Becker, K. H.; Fink, E. H.; Zabel, F. *J. Phys. Chem.* **1984**, *88*, 5020.
(11) Troe, J. *J. Phys. Chem.* **1979**, *83*, 114.
(12) Quack, M.; Troe, J. *Ber. Bunsen-Ges.* **1974**, *78*, 240.
(13) Cobos, C. J.; Troe, J. *J. Chem. Phys.* **1985**, *83*, 1010.
(14) Klippenstein, S. J.; Harding, L. B. *Phys. Chem. Chem. Phys.* **1999**, *1*, 989; *J. Phys. Chem. A* **1999**, *103*, 9388.
(15) Harding, L. B. *J. Phys. Chem.* **1989**, *93*, 8004; **1991**, *95*, 8653.
(16) Kuhn, B.; Rizzo, T. R.; Luckhaus, D.; Quack, M.; Suhm, M. A. *J. Chem. Phys.* **1999**, *111*, 2565.
(17) Harding, L. B.; Troe, J.; Ushakov, V. G. *Phys. Chem. Chem. Phys.* **2000**, *2*, 631.
(18) Harding, L. B.; Maergoiz, A. I.; Troe, J.; Ushakov, V. G. *J. Chem. Phys.* **2000**, *113*, 11019.
(19) Harding, L. B.; Stark, H.; Troe, J.; Ushakov, V. G. *Phys. Chem. Chem. Phys.* **1999**, *1*, 63.
(20) Harding, L. B.; Troe, J.; Ushakov, V. G. *Phys. Chem. Chem. Phys.* **2001**, *3*, 2630.
(21) Maergoiz, A. I.; Nikitin, E. E.; Troe, J.; Ushakov, V. G. *J. Chem. Phys.* **1998**, *108*, 5265.
(22) Maergoiz, A. I.; Nikitin, E. E.; Troe, J.; Ushakov, V. G. *J. Chem. Phys.* **1998**, *108*, 9987.
(23) Troe, J. *Chem. Phys. Lett.* **1985**, *122*, 425.
(24) Troe, J.; Ushakov, V. G. *Phys. Chem. Chem. Phys.*, to be published.
(25) Maergoiz, A. I.; Nikitin, E. E.; Troe, J.; Ushakov, V. G. *J. Chem. Phys.* **1996**, *105*, 6263.
(26) Maergoiz, A. I.; Nikitin, E. E.; Troe, J.; Ushakov, V. G. *J. Chem. Phys.* **1996**, *105*, 6277.
(27) Slater, N. B. *Theory of Unimolecular Reactions*; Methuen: London, 1959.
(28) Klippenstein, S. J.; Wagner, A. F.; Robertson, S. H.; Dunbar, R.; Wardlaw, D. M. *VariFlex*, http://chemistry.anl.gov/chem-dyn/variflex.
(29) Truhlar, D. G.; Garrett, B. C.; Klippenstein, S. J. *J. Phys. Chem.* **1996**, *100*, 12771.
(30) Wardlaw, D. M.; Marcus, R. A. *Chem. Phys. Lett.* **1984**, *110*, 230; *J. Chem. Phys.* **1985**, *83*, 3462. Robertson, S. H.; Wagner, A. F.; Wardlaw, D. M. *J. Chem. Phys.* **2000**, *113*, 2648.
(31) Benson, S. W. *Thermochemical Kinetics*, 2nd ed., Wiley: New York, 1976. Smith, G. P.; Golden, D. M. *Int. J. Chem. Kinet.* **1978**, *10*, 489.
(32) Troe, J. *J. Chem. Phys.* **1977**, *66*, 4745, 4758; *Annu. Rev. Phys. Chem.* **1978**, *29*, 223.
(33) Lenzer, Th.; Luther, K.; Reihs, K.; Symonds, A. C. *J. Chem. Phys.* **2000**, *112*, 4090. Grigoleit, U.; Lenzer, Th.; Luther, K.; Muetzel, M.; Takahara, A. *Phys. Chem. Chem. Phys.* **2001**, *3*, 2191.
(34) Troe, J. *Chem. Phys.* **1995**, *190*, 381.
(35) Salzgeber, R.; Mandelshtam, V. A.; Schlier, Ch.; Taylor, H. S. *J. Chem. Phys.* **1999**, *110*, 3756.
(36) Michael, J. V.; Su, M.-C.; Sutherland, J. W.; Carroll, J. J.; Wagner, A. F. *J. Phys. Chem. A* **2002**, *106*, 5297.
(37) Glaenzer, K.; Troe, J. *J. Chem. Phys.* **1975**, *63*, 4352. Quack, M.; Troe, J. *Ber. Bunsen-Ges.* **1977**, *81*, 329.
(38) Troe, J. *Ber. Bunsen-Ges.* **1974**, *78*, 478.
(39) Troe, J. *Ber. Bunsen-Ges.* **1983**, *87*, 161.
(40) Gilbert, R. G.; Luther, K.; Troe, J. *Ber. Bunsen-Ges.* **1983**, *87*, 169.
(41) Oref, I. *J. Phys. Chem.* **1989**, *93*, 3465. Pawlowska, Z.; Oref, I. *J. Phys. Chem.* **1990**, *94*, 567. Pawlowska, Z.; Gardiner, W. C.; Oref, I. *J. Phys. Chem.* **1993**, *97*, 5024.
(42) Wang, H.; Frenklach, M. *Chem. Phys. Lett.* **1993**, *205*, 271. Kazakov, A.; Wang, H.; Frenklach, M. *J. Phys. Chem.* **1994**, *98*, 10598.
(43) Prezhdo, O. *J. Phys. Chem.* **1995**, *99*, 8633.
(44) Venkatesh, P. K. *J. Phys. Chem. A* **2000**, *104*, 280.
(45) Troe, J.; Ushakov, V. G. *Faraday Discuss.* **2001**, *119*, 145.
(46) Troe, J. *Int. J. Chem. Kinet.* **2001**, *33*, 878.
(47) Hamon, S.; Speck, T.; Mitchell, J. B. A.; Rowe, B. R.; Troe, J. *J. Chem. Phys.* **2002**, *117*, 2557.
(48) Cobos, C. J.; Troe, J. *Z. Phys. Chem.* **2003**, *217*, 1031.
(49) Troe, J. *J. Chem. Phys.* **1983**, *79*, 6017.
(50) Olzmann, M.; Troe, J. *Ber. Bunsen-Ges.* **1992**, *96*, 1327; **1994**, *98*, 1563.
(51) Maergoiz, A. I.; Nikitin, E. E.; Troe, J.; Ushakov, V. G. *J. Chem. Phys.* **2002**, *117*, 4201.
(52) Dransfield, T. J.; Perkins, K. K.; Donahue, N. M.; Anderson, J. G.; Sprenguether, M. M.; Demerjian, K. L. *Geophys. Res. Lett.* **1999**, *26*, 687.
(53) Golden, D. M.; Smith, G. P. *J. Phys. Chem. A* **2000**, *104*, 3991.
(54) Brown, S. S.; Talukdar, R. K.; Ravishankara, A. R. *Chem. Phys. Lett.* **1999**, *299*, 277.
(55) D'Ottone, L. D.; Campuzano-Jost, P.; Bauer, D.; Hynes, A. J. *J. Phys. Chem. A* **2001**, *105*, 10538.
(56) Donahue, N. M.; Dubey, M. K.; Mohrschladt, R.; Demerjian, K. L.; Anderson, J. G. *J. Geophys. Res.* **1997**, *102*, 6159.
(57) Hippler, H.; Nasterlack, S.; Striebel, F. *Phys. Chem. Chem. Phys.* **2002**, *4*, 2959.
(58) Hippler, H.; Rahn, R.; Troe, J. *J. Chem. Phys.* **1990**, *93*, 6560.
(59) Baer, S.; Hippler, H.; Rahn, R.; Siefke, M.; Seitzinger, N.; Troe, J. *J. Chem. Phys.* **1991**, *95*, 6463.
(60) Luther, K.; Stark, H.; Troe, J. *16th International Gas Kinetics Symposium*, Cambridge, England, 2000. Bloss, W. J.; Nickolaisen, S. L.; Salawitch, R. J.; Friedl, R. R.; Sander, S. P. *J. Phys. Chem. A* **2001**, *105*, 11226.

CR020514B